ROMANIA

MINISTRY OF NATIONAL DEFENSE

MILITARY TECHNICAL ACADEMY „FERDINAND I”

FACULTY OF COMMUNICATIONS AND ELECTRONIC SYSTEMS FOR DEFENSE AND SECURITY

MASTER PROGRAM: COMMUNICATION SYSTEMS ENGINEERING AND ELECTRONIC SECURITY

”THE ANALYSIS OF SIGNALS FROM ULTRA-WIDEBAND SYSTEMS”

”ANALIZA SEMNALELOR PROVENITE DIN SISTEME UWB”

Coordinating professor:

Cpt. conf. univ. dr. ing. Angela DIGULESCU-POPESCU

Master student:

Slt.ing. Paraschiva-Cristina POPOVICI

Bucharest 2022

Chapter 1

1.1 Introduction

Surveillance, safety and security are important aspects of human-machine interaction in hospitals [20], perceptive car scenarios, smart factories, and so on. Detection and localization techniques, such as computer vision, infrared detectors, LADAR (Laser Detection and Ranging) signatures, UWB radar [21], Global Positioning System (GPS), vibration and seismic sensors, and acoustic sensors [20] were recently developed for ensuring human safety by detection and localization of moving persons or objects, and not only.

In the last 20 years, UWB technology has been developed for high data rate communications, radar communications, surveillance and safety applications, indoor localization, through-wall radar applications and other niche applications. UWB is used in Personal Area Networks, having a short coverage area of approximately 10 meters [22].

Line of sight (LOS) [23] , bad weather conditions, environmental interference and privacy issues [24] could degrade and prevent the performance of enumerated technologies, except for UWB radar, which is appropriate for any kind of environment due to its high range resolution [21] and noise robustness.

1.2. UWB technology theoretical concepts

UWB technology is a wireless technology, used in WPAN (Wireless Personal Area Network) networks, introduced due to the need for higher data transfer speed (Mbps, Gbps) [2].

UWB signals are very short-term pulses (ns), occupying a wide spectrum. The unlicensed spectrum allocated for the ultra-wideband devices (UWB) is within the 3.1 GHz – 10.6 GHz frequency range, occupying the 7.5 GHz bandwidth [3]. A device is considered ultra-wideband if the fractional bandwidth is -10 dB or more than 20% of the central frequency [4]. Its large bandwidth makes this technology suitable for localization and tracking applications, providing high temporal resolution.

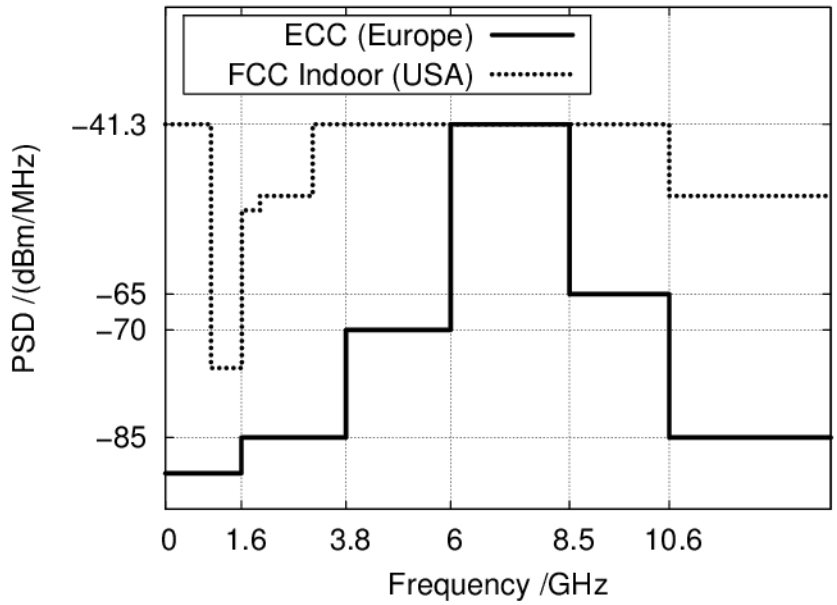

Figure 1 FCC and ECC mask limitations [25]

The Federal Communications Commission (FCC) and Electronic Communications Committee (ECC) mask limitations concerning transmission power limitations and allocated bandwidth. These limitations are imposed to avoid interference with other devices. In Romania, the regulatory regime for UWB technology is ECC Rec 70-03 /ECC Decision 06(04) / ETSI EN 302 065, which permits a frequency range of 3.1 – 4.8 GHz, 6.0 – 8.5 GHz and 8.5 – 9.0 GHz. The maximum equivalent isotropic radiated power (EIRP) is -41.3 dBm/ MHz [26].

One of the advantages of this technology is the low consumption of resources, using a very low emission power (P_t < 0.5 mW). A signal that occupies a

very wideband and uses a very low transmission power is similar to noise in the time domain, being resistant to jamming, providing a low probability of interception and detection, and being advantageous for secret military applications [27].

An UWB radar can be used for security, rescue and surveillance applications [28], providing a good range resolution, which makes it a suitable technique for human movement detection [20].

An UWB radar transmits a series of short-term, low-power pulses [29], which are reflected by the environment, travel a round trip distance, later received by the radar receiver [30]. The radar echo signal is analyzed for human or object detection [29]. The characteristics of the target are given by the changes in the properties of the echo signal [31].

1.3 Channel estimation

The UWB communication is influenced by the propagation channel, causing multipath propagation [32]. Phenomena such as reflection, diffraction, and absorption are due to the interaction of the emitted pulse with different objects in the environment in which the system operates. Each interaction can cause direction changing and delays, and this leads to splitting up the components into new ones [33]. For UWB systems, due to their large bandwidth, the free-space attenuation, and the effect of diffraction, reflection at dielectric walls are frequency-dependent [34].

The multipath components have a delay, an attenuation and a direction of arrival, depending on the path they take. Differentiating the channel propagation conditions (LOS/NLOS) is important for applications such as indoor localization or vehicle-to-vehicle communication [35].

The propagation channel has a different effect on UWB signals in comparison to narrowband signals, due to their large bandwidth. The path gain of

the received signal is frequency-dependent, as well as the time delays of the clusters and rays. A cluster is a group of multipath components, due to the multipath propagation.

The main standard which describes the channel estimation is IEEE 802.15.4a. There are ten proposed channel models, based on the change of the specific parameters due to the environmental conditions and the other channel effects.

Table 1. IEEE 802.15.4a Channel models

Channel Number	Environments	Propagation
CM1	Indoor residential	LOS
CM2	Indoor residential	NLOS
CM3	Indoor office	LOS
CM4	Indoor office	NLOS
CM5	Outdoor	LOS
CM6	Outdoor	NLOS
CM7	Industrial	LOS
CM8	Industrial	NLOS
CM9	Open outdoor	NLOS
BAN	Body area network	NLOS

The channel model proposed by IEEE 802.15a is derived from the Saleh-Valenzuela model which states that the received signal is composed of clusters and rays, each having independent fading, meaning attenuated and delayed versions of the transmitted signal. The arrival times of clusters and rays follow a Poisson distribution [36], where the multipath gain magnitude follows a log-normal distribution [22].

The received signal is considered as:

$$r(t) = \int_{-\infty}^{\infty} c(t,\tau)w(t-\tau)d\tau + n(t) \quad (1)$$

Where the terms represents:

τ : the delay

$n(t)$: the additive Gaussian noise

$w(t-\tau)$: the delayed version of the emitted signal

$c(t,\tau)$: the channel impulse response which is a time-variant

The channel impulse response equation is given as follows:

$$c(t) = \sum_{c=1}^{C} \sum_{r=1}^{R_c} a_{cr} \delta(t - T_c - \tau_{cr}) \quad (2)$$

Where the terms represents:

C : the number of clusters (groups of multipath rays arriving in the receiver)

R_c : the number of multipath components of the cluster

T_c : the arrival time of each cluster

τ_{cr} : the arrival time of each multipath component in the cluster

δ : Dirac delta function

a_{cr} : the multipath gain coefficient

The path gain describes the average attenuation of the signal transmitted from the emitter Tx to the receiver Rx, which depends on the distance between the emitter and the receiver [33].

The number of multipath components which can occur within a cluster depends on the environment, more objects in the environment and a larger excess delay can determine more multipath components (MPCs), a large bandwidth

reduces the number of MPCs per delay bin [33]. The increasing delay determines the increase of fading.

Depending on the environment and propagation conditions, channel impulse response may affect the signal propagation differently, some examples of channel impulse response in the industrial environment with LOS and NLOS propagation and their energy-delay profiles are given in the images below:

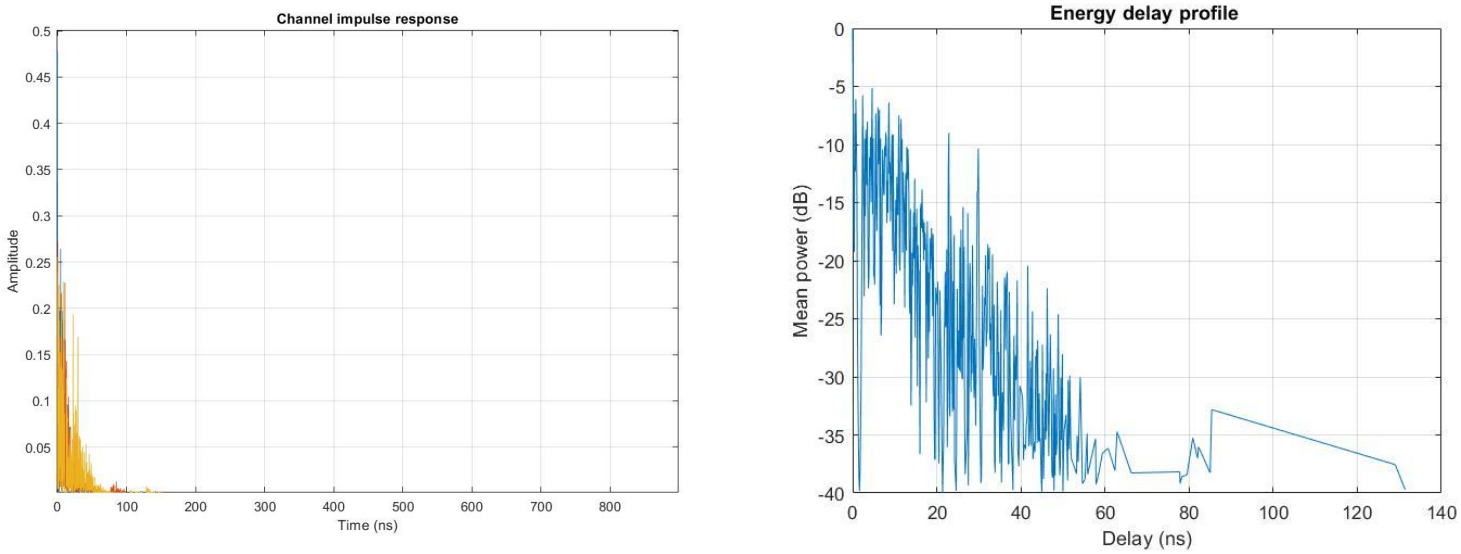

Figure 2 CM3 Indoor office (Line of Sight)

The channel impulse response acts as a filter upon the emitted signal, thus Non-Line of Sight propagation conditions determines a greater effect on the transmitted signals, phenomena such as reflections and diffraction are determined by the objects between the emitter and the receiver. Data need to be preprocessed at the receiver side to distinguish the desired signal from the clutter and noise.

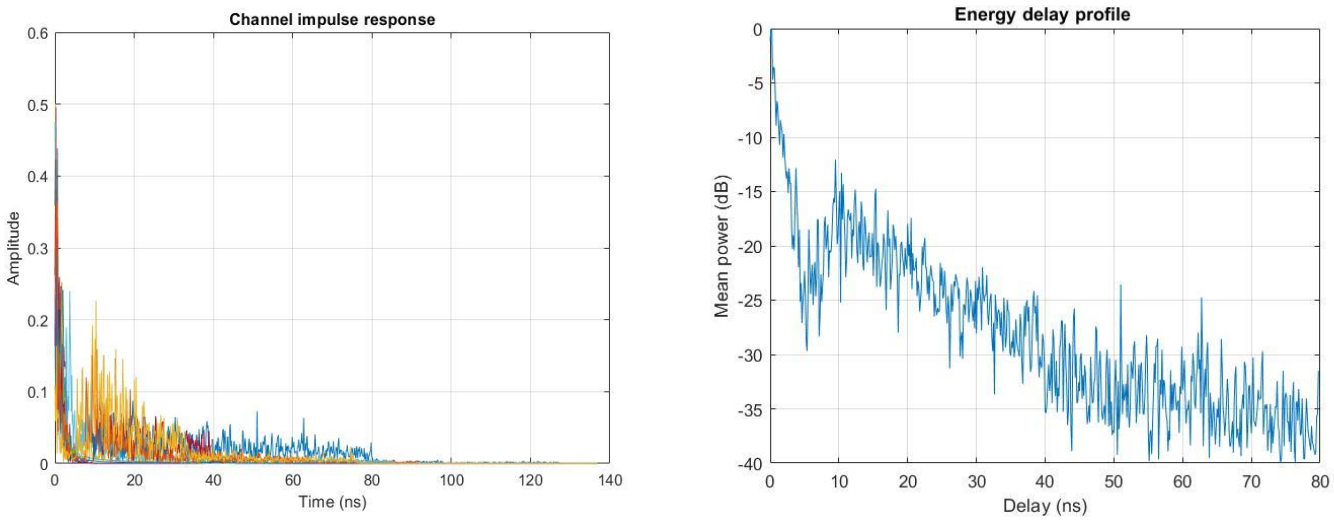

Figure 3. CM7 Industrial (Line of Sight)

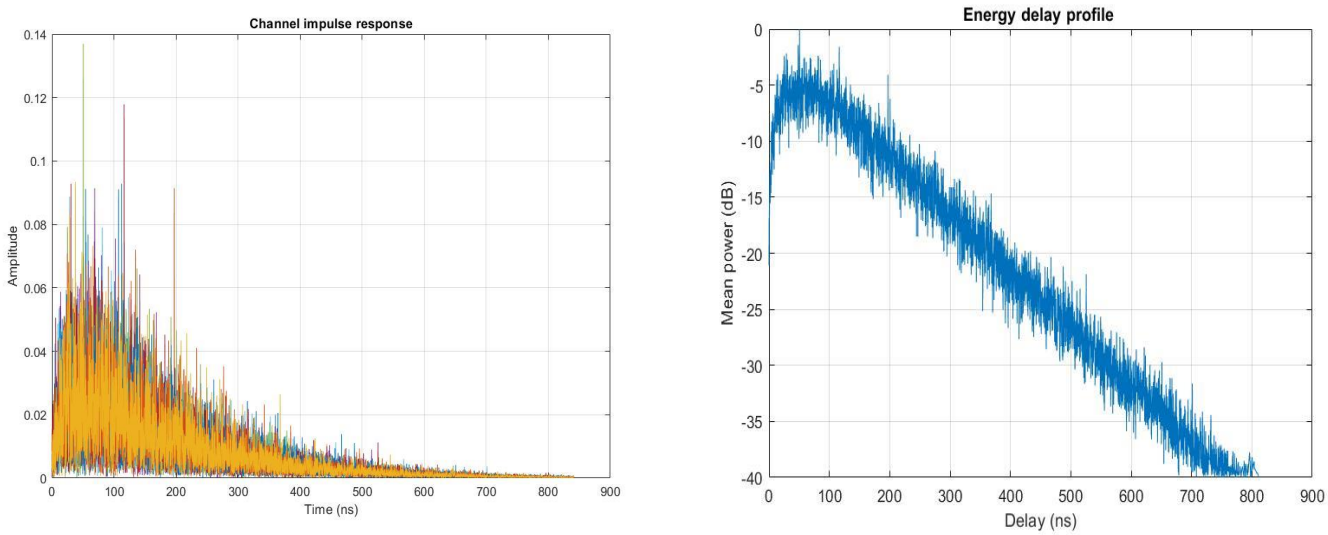

Figure 4 CM8 Industrial (Non-Line of Sight)

30 din

Chapter 2

UWB Signal Processing Methods

The objectives of this chapter are to present some signal processing techniques for UWB signals and channel estimation, such as envelope detection via Hilbert Transform for signal period estimation, Power Spectral Density Estimation via Welch Method for determining the signal bandwidth, Matched filter for the signal to noise ratio maximizing, Search Subtract and Readjust method for multipath components extraction.

2.1. Envelope Detection using Hilbert Transform

The signal envelope detection could have application in finding the period of a signal, in imagery classification, in application for positioning and others. To determine the envelope of the original waveform $g(t)$, the absolute value of the analytic signal is used [37]. The analytical signal is composed of the original signal and its Hilbert Transform and has no negative frequency components.

Given a signal $g(t)$, the absolute value of the analytic signal $G_a(t)$, which is composed of the original waveform $g(t)$ and its Hilbert transform $\tilde{g}(t)$, can be used to determine the signal's envelope:

$$G_a(t) = g(t) + i\tilde{g}(t) \tag{3}$$

The Hilbert Transform presumes that the original signal is filtered by a filter with an impulse response function of $h(t) = \frac{1}{\pi t}$.

$$\tilde{g}(t) = g(t) * \frac{1}{\pi t} \tag{4}$$

In the frequency domain, the expression of the Hilbert Transform of $g(t)$ will be as follows:

$$F\{\hat{g}(t)\} = [G_{-}(f) + G_{+}(f)]\big(-j\,\mathrm{sgn}(f)\big) = jG_{-}(f) - jG_{+}(f) \quad (5)$$

The analytic signal is constructed by suppressing all the negative frequency of the real signal and can be written as:

$$G_a(f) = G_{-}(f) + G_{+}(f) + j[jG_{-}(f) - jG_{+}(f)] \quad (6)$$

$$G_a(f) = 2\,G_{+}(f) \quad (7)$$

The envelope detection is performed using the absolute value of the analytical signal.

2.2 Power Spectral Density Estimation via Welch's method

"Power Spectral Density describes the power of a signal or time series distributed over different frequencies" [38] .

The Discrete Fourier Transform of the autocorrelation of a signal $x(t)$ is called the Power Spectral Density (PSD) [38], where $R_{xx}(k)$ is the autocorrelation function of the signal $x(t)$.

$$S_{xx}(f) = \sum_{k=-\infty}^{\infty} R_{xx}(k)e^{-i\omega kT} \quad (8)$$

Welch's method requires the segmentation of a time series of length N in L overlapped segments of length M, multiplied by an established window function, then computing DFT on each segment:

$$x_m(n) = w(n)x(n + mR) \quad (9)$$

Where:

$n = 0..M-1$ represents the window length

$m = 0,1,\ldots K-1$ the m′th windowed frame

R : window hop size

K : the available frames

Welch's estimate of Power Spectral Density is given as follows:

$$S_x^W(f) = \frac{1}{K}\sum_{m=0}^{K-1} P_{x_{m,M}}(f) \tag{10}$$

Where:

$$P_{x_{m,M}}(f) = \frac{1}{M}\left|\sum_{n=0}^{N-1} x_m(n)e^{-j2\pi nk/N}\right|^2 \tag{101}$$

The window function such as Rectangular window, Barlett window, Hanning window, Hamming window or Blackman window [38] are used for PSD estimation via Welch's method.

To determine the bandwidth of interest for the reference UWB signal, a PSD estimation via Welch's Method is computed, using a Hamming window function of an input signal period`s length, with 0 overlap samples for better noise reduction in the estimated power spectrum. The Hamming window function is the following:

$$W(n) = \begin{cases} 0.54 + 0.446\cos\left(\frac{2\pi n}{N}\right), |n| < \frac{N-1}{2} \\ 0, \text{otherwise} \end{cases} \tag{11}$$

2.3 Baseband Conversion

To convert a signal to the baseband requires the multiplication of the input signal with a reference signal having the same central frequency f_c, then a low pass filtration at the cutoff frequency f_{cutoff} equal to the subtraction of the upper frequency and the central frequency.

$$f_c = f_{upper} - \frac{BW}{2} \quad (12)$$

$$f_{cutoff} = f_{upper} - f_c \quad (13)$$

Where

f_{upper} : the upper frequency of the input signal

BW : the input signal's frequency bandwidth

2.4 Matched Filter

Matched filters are designed to maximize the signal to noise ratio (SNR) of an input signal. This is accomplished by the convolution of the signal with the template waveform, which is the time reverse input signal [39].

Given an input signal $(t) = x(t) + n(t)$, where $x(t)$ is the signal of interest and $n(t)$ is the noise, the maximum SNR at the output will occur when the filter has an impulse response that is time-reverse of the input signal [39].

The convolution of this impulse response with the signal $x(t)$ provides the autocorrelation in the input signal. The matched filter is defined by an impulse response which corresponds to the reverse time reference signal, as:

$$h(t) = x(T - t) \tag{14}$$

where T is the period of the template signal.

2.5 Search Subtract and Readjust

The received UWB signal will be a sum of attenuated and delayed versions of the ideal reference emitted signal, due to the multipath propagation, according to the Saleh Valenzuela model. The propagation channel acts as a filter, so to estimate the multipath components, channel impulse response needs to be estimated.

A method for channel estimation and determination of Time of Arrival and the amplitudes of the multipath components is Search Subtract and Readjust method, proposed in [40].

Let $c(t)$ be the channel impulse response, with c_l and τ_l the amplitudes and delays of the L multipath components [40]:

$$c(t) = \sum_{l=1}^{L} c_l \delta(t - \tau_l) \tag{15}$$

Let $w(t)$ be the ideal received pulse, $n(t)$ the additive Gaussian noise and $r(t)$ the received signal:

$$r(t) = \sum_{l=1}^{L} c_l w(t - \tau_l) + n(t) \tag{16}$$

The additive Gaussian noise has zero mean and $\frac{N_0}{2}$ spectral density. The c_l and τ_l parameters, $l = 1 \dots L$, characterize the channel impulse response.

The length of the ideal emitted signal is Z, the length of the received signal is M , where $Z < M$. The received signal is written as a vector:

$$r = W(\tau)c + n \tag{17}$$

Where $W(\tau) = [w^{(D_1)}, w^{(D_2)} \dots . w^{(D_l)}]^T \in R^{MxL}$ represents the matrix of the delayed versions of $w(t)$ and $w^{(D_l)} = [0_{D_l}, w, 0_{M-Z-D_l}]^T$, with D_l the discretized version of time delay τ_l.

The amplitudes and delays are iteratively estimated, based on the subtraction of the first found path from the received signal, resulting in the residual signal.

The signal to noise ratio of the residual signal is iteratively maximized by a matched filter. The parameters for the strongest path are estimated from the absolute output values of the Matched Filter.

The estimated delay is determined by suppressing the matched filter delay, thus by the difference of the sample corresponding to the largest peak k_1 and the length Z of the ideal waveform $w(t)$.

$$\hat{\tau}_{k_1} = k_1 - Z \tag{18}$$

The amplitude estimate $\hat{c}_{k_1}$ of the strongest path is calculated as :

$$\hat{c}_{k_1} = (w^{(k_1)^T} w^{(k_1)})^{-1} \; w^{(k_1)^T} r \tag{19}$$

Where $(w^{(k_1)^T} w^{(k_1)})^{-1} \; w^{(k_1)^T}$ is the pseudoinverse matrix of $w(\tau_{k_1})$.

The residual signal r' results by subtracting the current strongest path from the received signal and the algorithm is repeated until all the paths are found.

$$r' = r - \hat{c}_{k_1} w^{(k_1)} \tag{20}$$

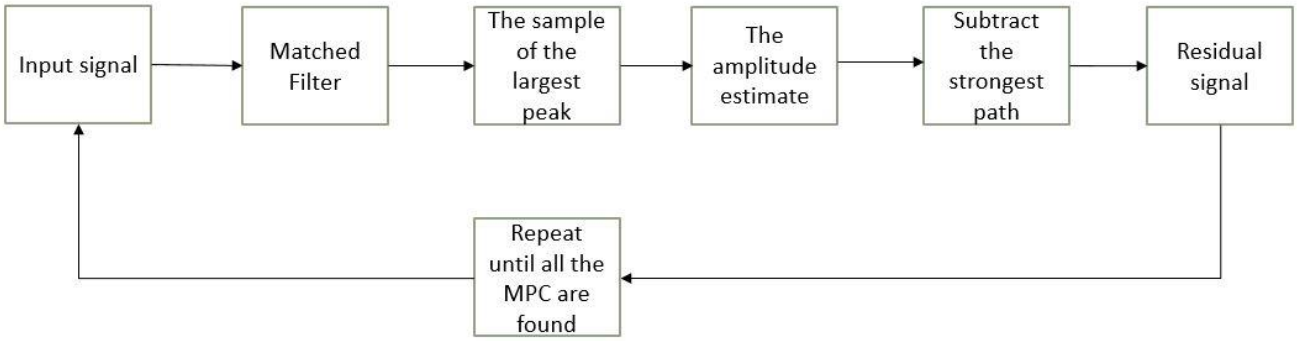

Figure 5 Steps of the algorithm

2.5.1 SSR Model Validation

The SSR model validation is performed on synthetic signals, the channel impulse response being given as reference. The generated waveform is the second Gaussian derivate $g(t)$, where t represents the fast time and t_p represents the pulse width.

$$g(t) = \frac{1}{\sqrt{2\pi}}\left(1 - \frac{t^2}{{t_p}^2}\right) e^{\frac{-1}{2}\frac{t^2}{{t_p}^2}} \tag{21}$$

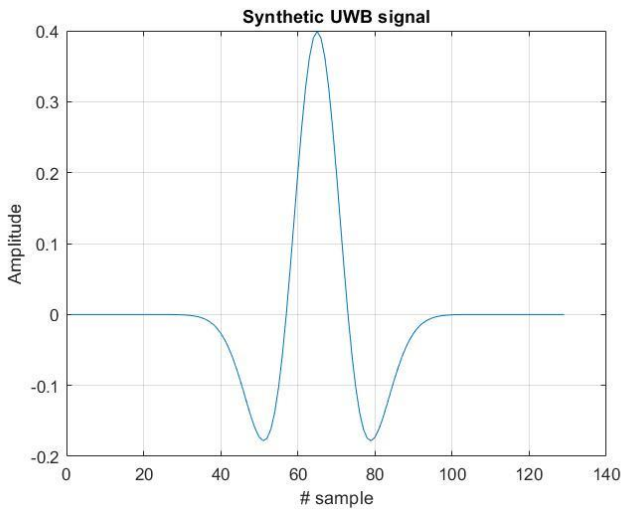

Figure 6 Second Gaussian derivate waveform

The bias of an estimator represents the difference between the average of the estimated values and the original ones, and the variance tells us how spread the data are.

$$\text{Bias}(x|\theta) = \mathrm{E}_{x|\theta}[\hat{\theta} - \theta] \tag{22}$$

$$\text{Variance}(\theta) = \mathrm{E}[(\hat{\theta} - \mathrm{E}[\hat{\theta}])^2] \tag{23}$$

Where

θ : the true values

$\hat{\theta}$: the estimated values

E : the expected value (the mean value)

To calculate the biases and the variances for the parameters estimates, an interval of SNR values of [-10, 0], where 1000 Monte Carlo trials are considered.

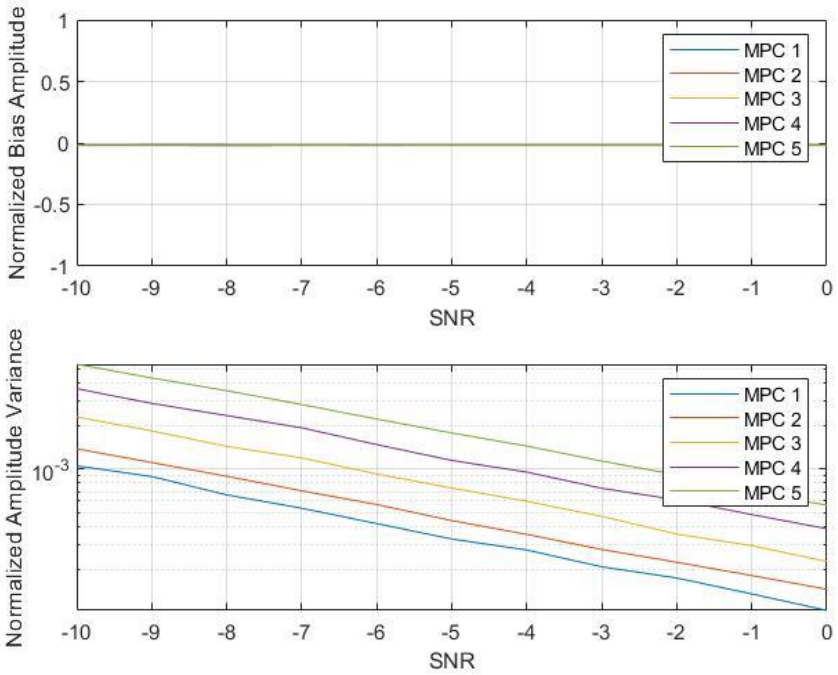

Figure 7 Biases and variances for the amplitudes

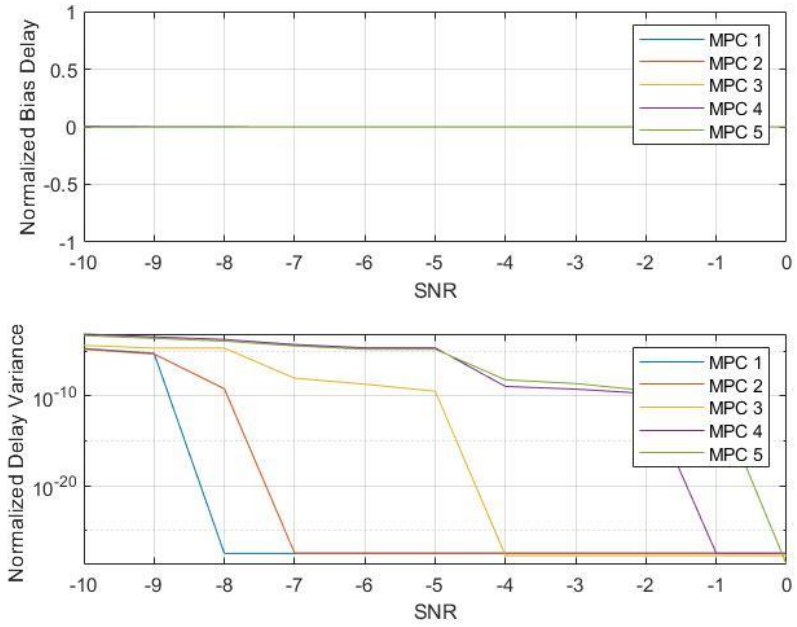

Figure 8 Biases and variances for the delay estimates

The delay estimator is unbiased and the variances decrease, SNR does not affect the delay estimation, due to the matched filter. Regarding the amplitudes, they are directly affected by the SNR. The edge of the normalized histogram is compared to a Weibull Distribution probability density function and the Normal Distribution probability density function, and it is observed that amplitude estimates follow a Normal Distribution, an observation validated by Chi-squared and Kolmogorov Smirnov statistical tests.

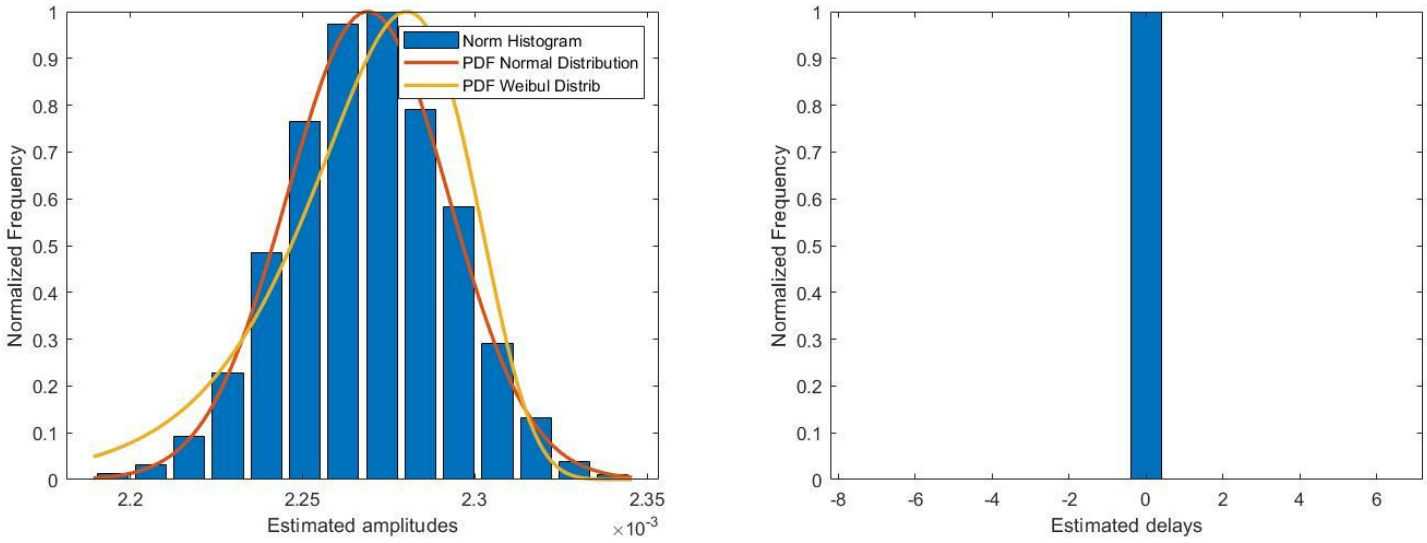

Figure 9 The normalized histograms for amplitudes and delays

The delays seem to follow a uniform distribution, thus the impact of the signal to noise ratio is less powerful than in the case of the amplitudes, due to the use of the matched filter.

Kolmogorov Smirnov test relies on the distance between the two curves in the figure above, which represents the empirical cumulative distribution function of our data and the normal distribution cumulative distribution function.

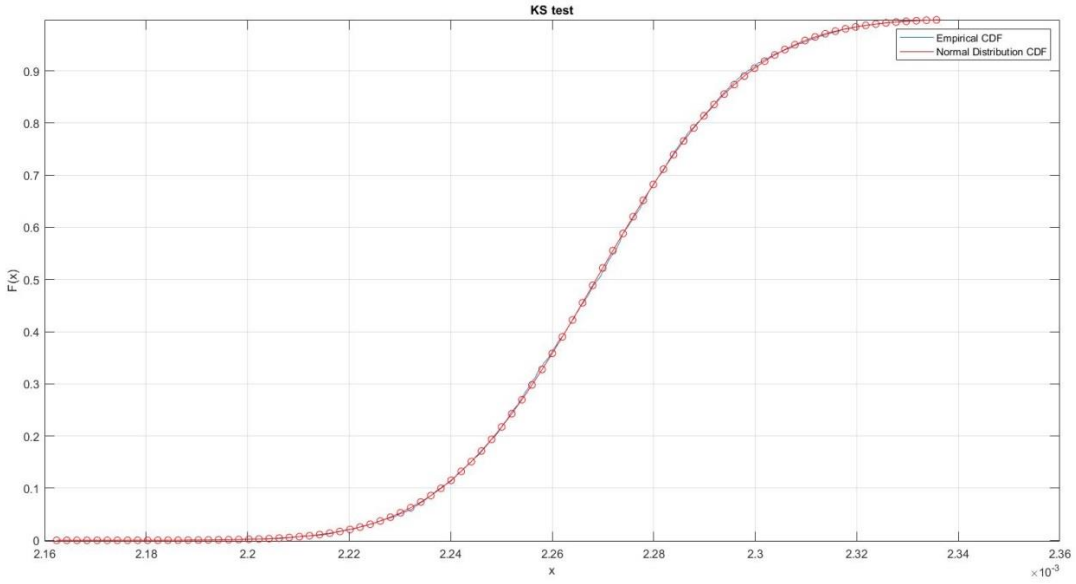

Figure 10. Kolmogorov Smirnov test

To determine the estimator's performance and efficiency, the variances are compared to the Cramer Rao Lower Bound, which is the lowest bound of the variance of an unbiased estimator.

The Normal distribution probability density function:

$$f(x) = \frac{1}{\sigma\sqrt{2\pi}} e^{-\frac{1}{2}\left(\frac{x-\mu}{\sigma}\right)^2} \tag{24}$$

where μ is the mean of data and σ is the standard deviation of the noise.

The Cramer Rao Lower Bound variance:

$$\sigma_{CR}^2 = -\left[\frac{\partial^2}{\partial^2 \mu} \ln\left(f(x,\mu)\right)\right]^{-1} =$$

$$= -\left[\frac{\partial \ln\left(f(x,\mu)\right)}{\partial \mu}\left(\ln\left(\sigma\sqrt{2\pi}\right) + \frac{(x-\mu)^2}{2\sigma^2}\right)\right]^{-1} = -\left[\frac{-1}{\sigma^2}\right]^{-1} = \sigma^2 \tag{25}$$

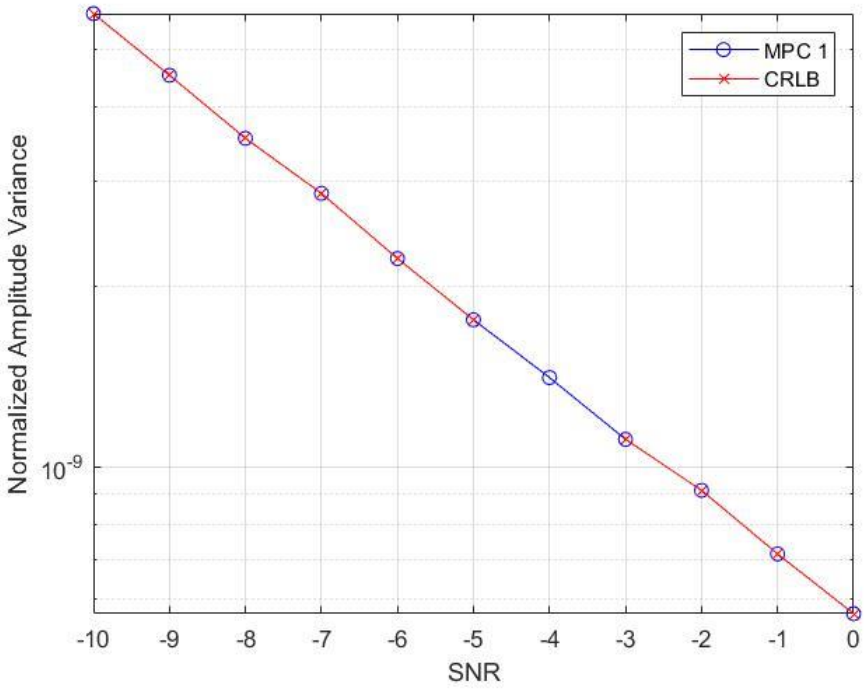

Figure 11 CRLB and Variances of the first MPC

The efficiency of the estimator is given by the ratio of the Cramer Rao Lower Bound and the variance of the estimator, which is almost equal to one.

4.1 Signal processing methods for UWB signals

For the analysis of the signals from UWB systems, the communication system is considered as follows:

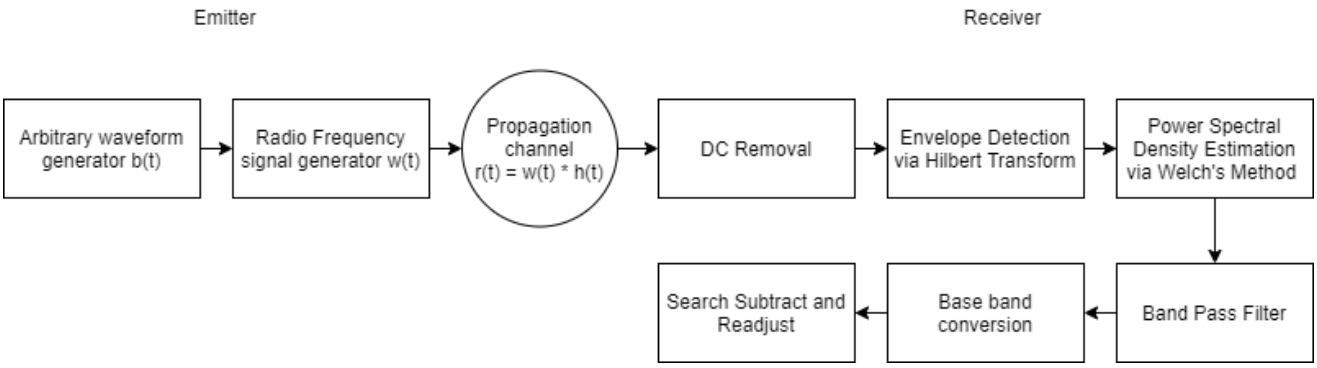

Figure 26 Communication system

The emission system proposed in our case for UWB signal generation is composed of two signal generators:

- an arbitrary waveform generator
- a radiofrequency generator.

An arbitrary waveform generator can generate any given wave shape given by the user. The arbitrary waveform generator emits the ideal UWB baseband signal with a 5 ns pulse duration and a 2 GHz bandwidth. The radiofrequency generator translates the baseband UWB signal on a central frequency of 7.25 GHz. The resulted signal is a training impulse with a 90 ns signal period, occupying a 2 GHz frequency bandwidth.

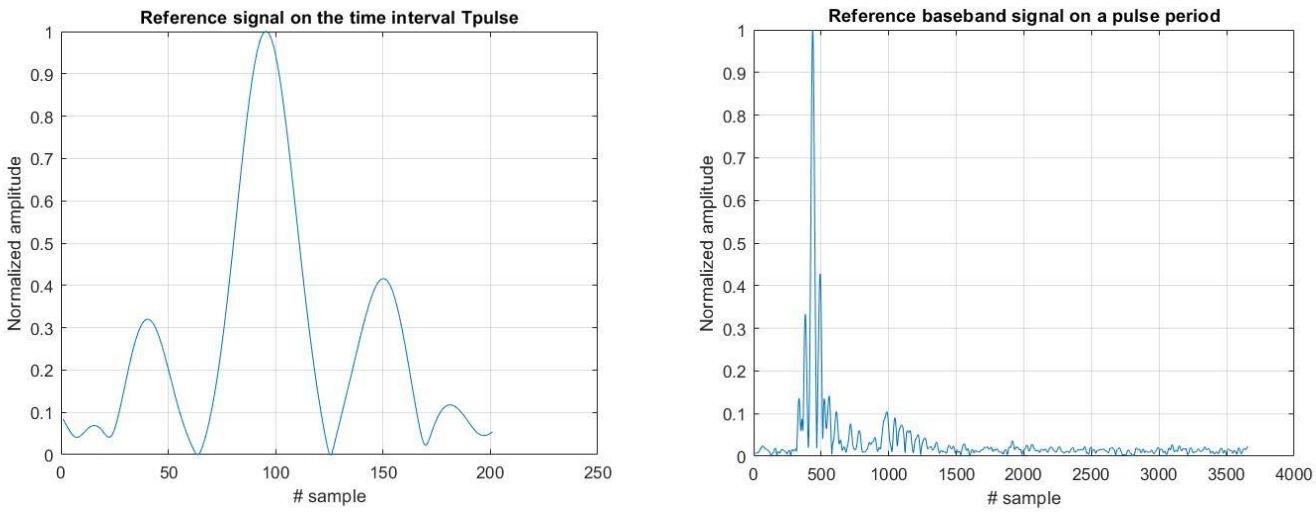

Figure 27 The reference UWB baseband signal

The signal is received using a high sampling rate oscilloscope at a sampling frequency of 40 GHz, concerning the Nyquist Rate. The effect of the propagation channel and the background noise on the wireless signal is observed in the signal to noise ratio, which is much lower in the wireless channel.

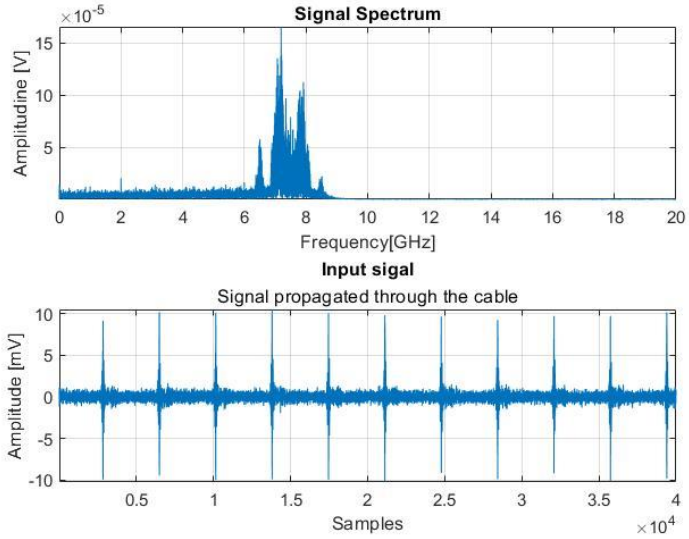

Figure 28 a. Cable signal and its spectrum

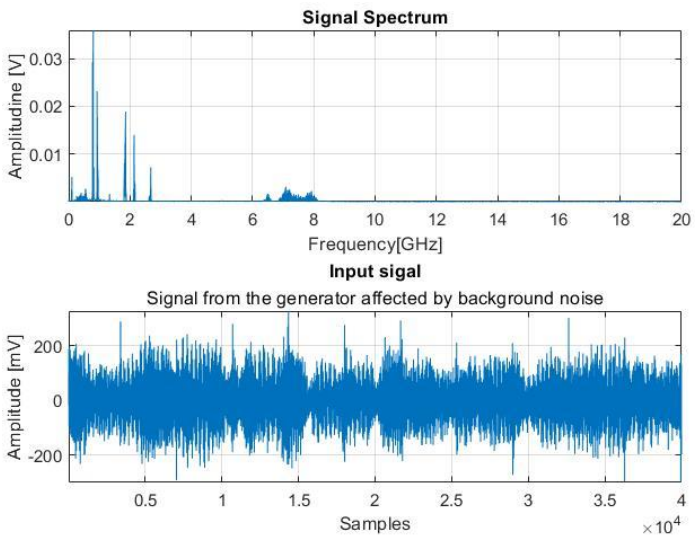

b. Wireless signal and its spectrum

The envelope detection if performed on the received signal, where the number of the signal envelope`s peaks, using a threshold of 75% of the maximum amplitude value, corresponds to the number of the signal's periods. The length of a period is the division of the total signal length and the number of periods.

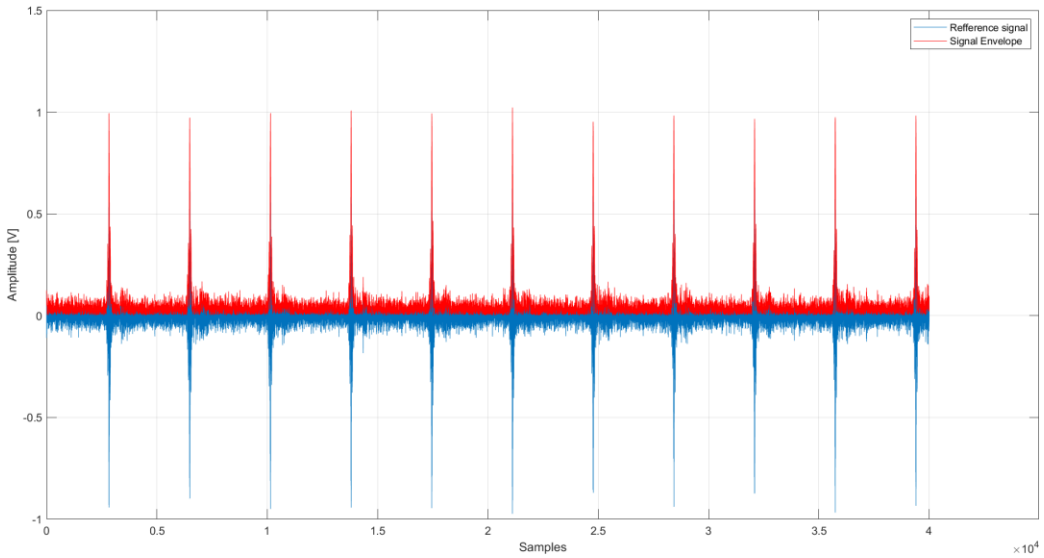

Figure 29 The original waveform and its envelope using the Hilbert transform

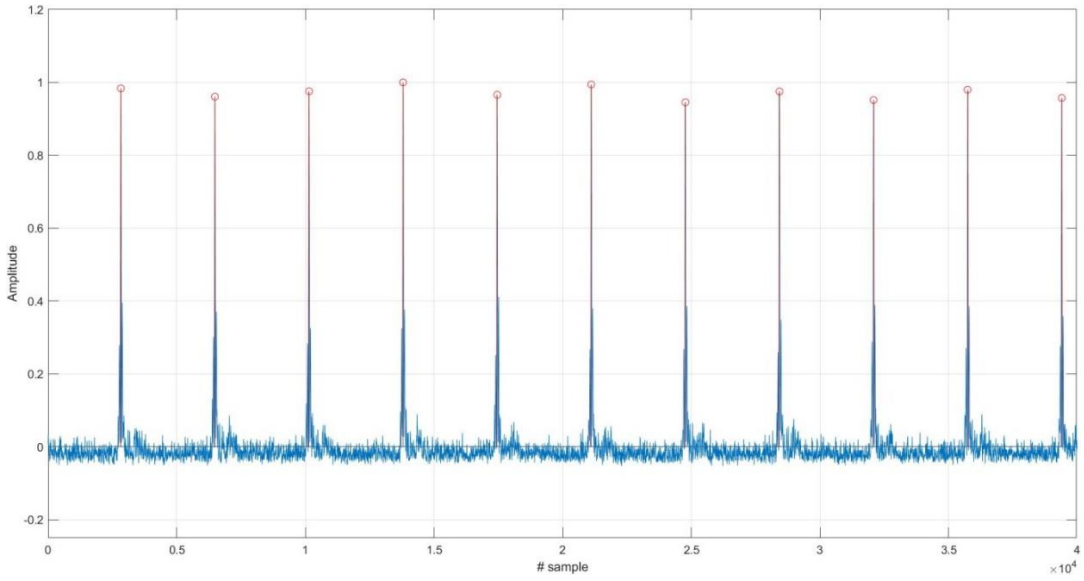

Figure 30 Finding the peaks of the signal envelope concerning a 75% threshold

To find out the signal's bandwidth, Power Spectral Density via Welch's method is performed. A bandwidth of 2 GHz is observed in the representation of the Power Spectral Density, with a central frequency of 7.25 GHz, by using a fixed threshold.

Using the 2 GHz bandwidth, a digital bandpass filter is used for filtering the input signal, having an upper frequency of 8.25 GHz and the lower frequency of 6.25GHz.

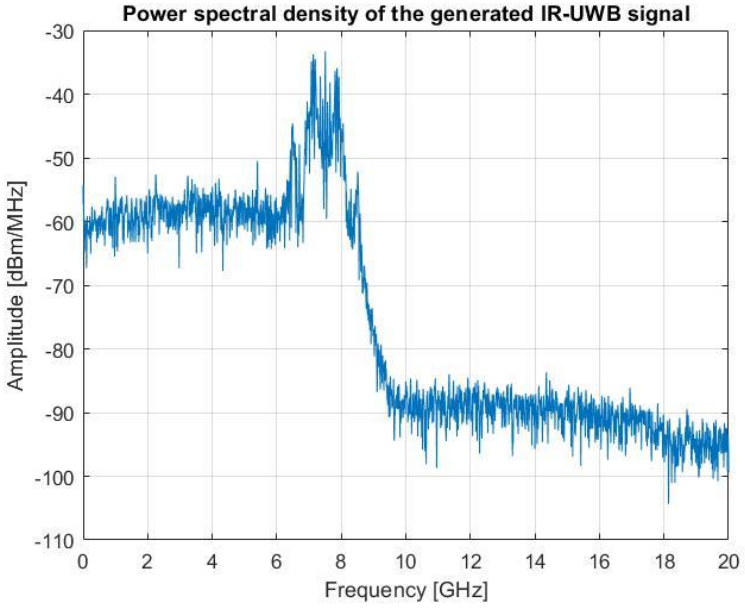

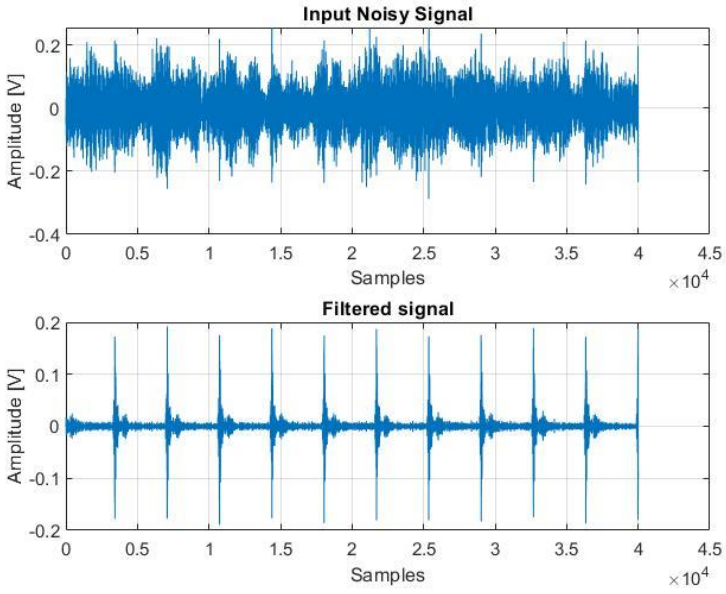

Figure 31 a. Power Spectral Density of the generated signal b. The filtered generated signal

The input signal will be converted in the baseband with the use of a frequency mixer, followed by a low pass filter, for further numerical signal processing.

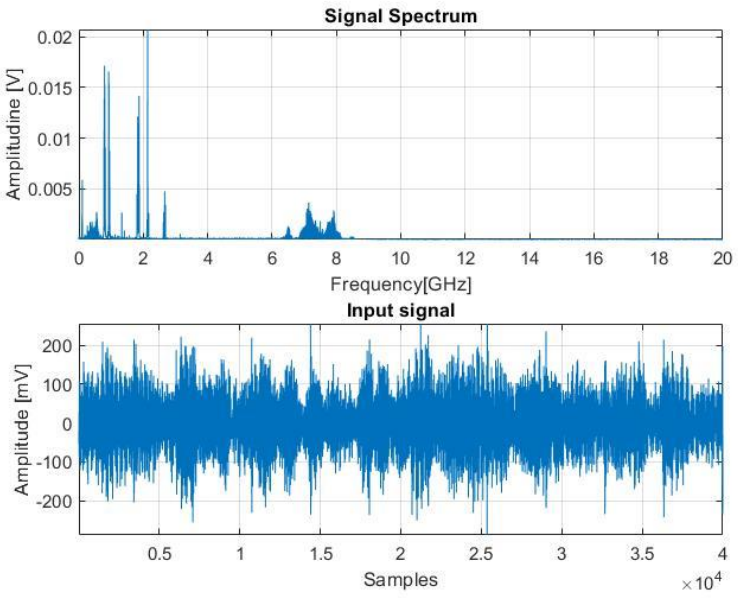

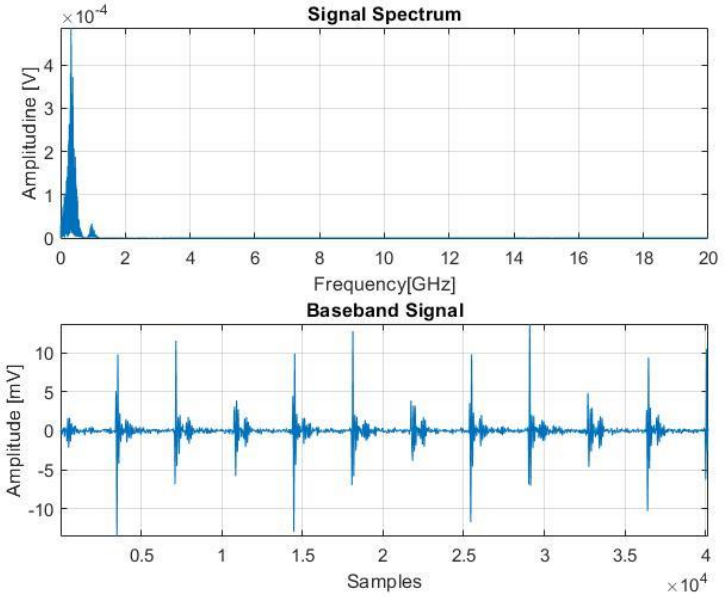

Figure 32. a. The original signal and its frequency spectrum b.The baseband signal and its frequency spectrum

To maximize the SNR and filter the UWB signal, a matched filter based on the time-reversed ideal baseband emitted signal is designed, and then the convolution between the input signal and the filter's impulse response is computed, SNR being maximum at the signal's period. The Matched Filter introduces a delay equal to the length of the reference signal, which must be suppressed for further time delay estimation of the multipath components.

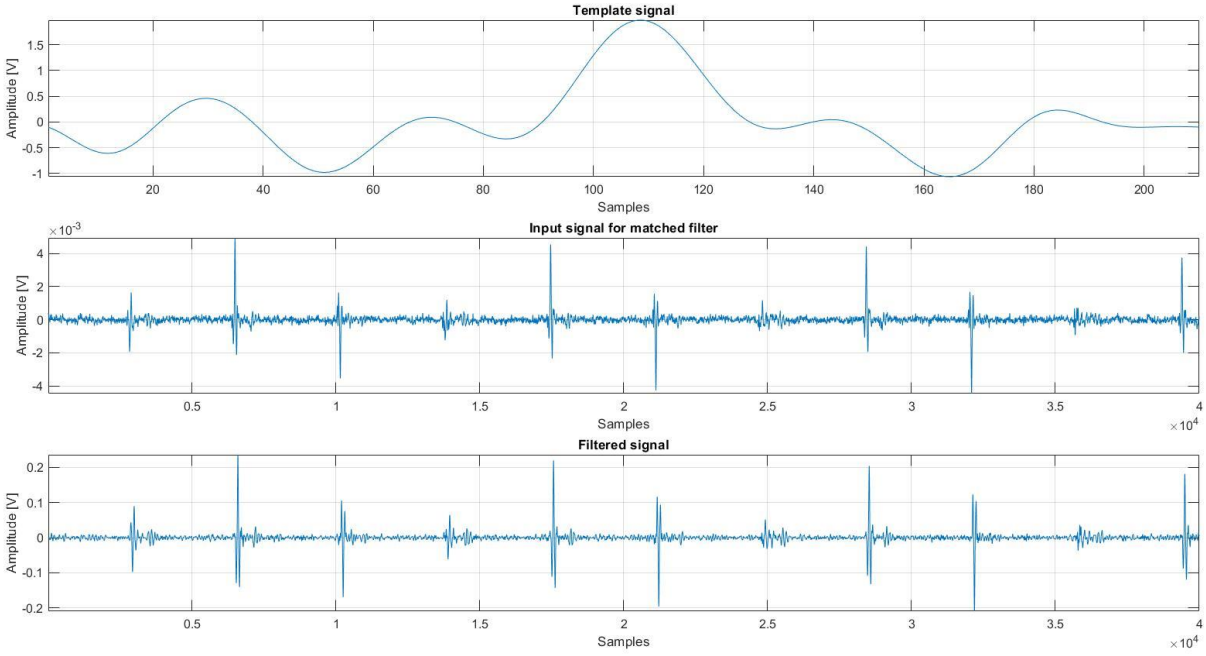

Figure 33. Template signal, input signal and the matched filter`s output

After applying the matched filter, the Search Subtract and Readjust algorithm was applied on a period of the signal to extract the multipath components. In the figure below, a period of the resulted signal in the time domain is presented:

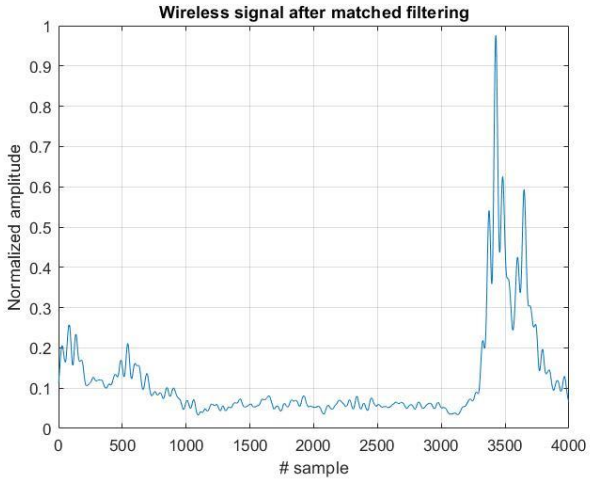

Figure 34. Wireless Signal after Matched Filter

SSR is based on the iterative correlation of the template waveform with the input signal and determines the set of amplitude and delay parameters, then extracting the template waveform with these parameters from the original signal.

The SSR method extracts the multipath components from the received signal and iteratively maximizes the signal to noise ratio and improves the time resolution in the signal, compared to Matched Filter, which maximizes the signal to noise ratio just once.

It is observed that there are three multipath components on a signal period, from which two are superposed, having a small-scale fading, due to the multipath propagation. Also, the strongest path is not always the first ray that arrives at the receiver and the later the rays arrive, the lower power they have. The time of arrival of the received signal is considered to be the moment when the first ray arrives at the receiver. Time of arrivals of the multipath components can be utilized in the positioning application, thus SSR could be an effective algorithm in this matter.

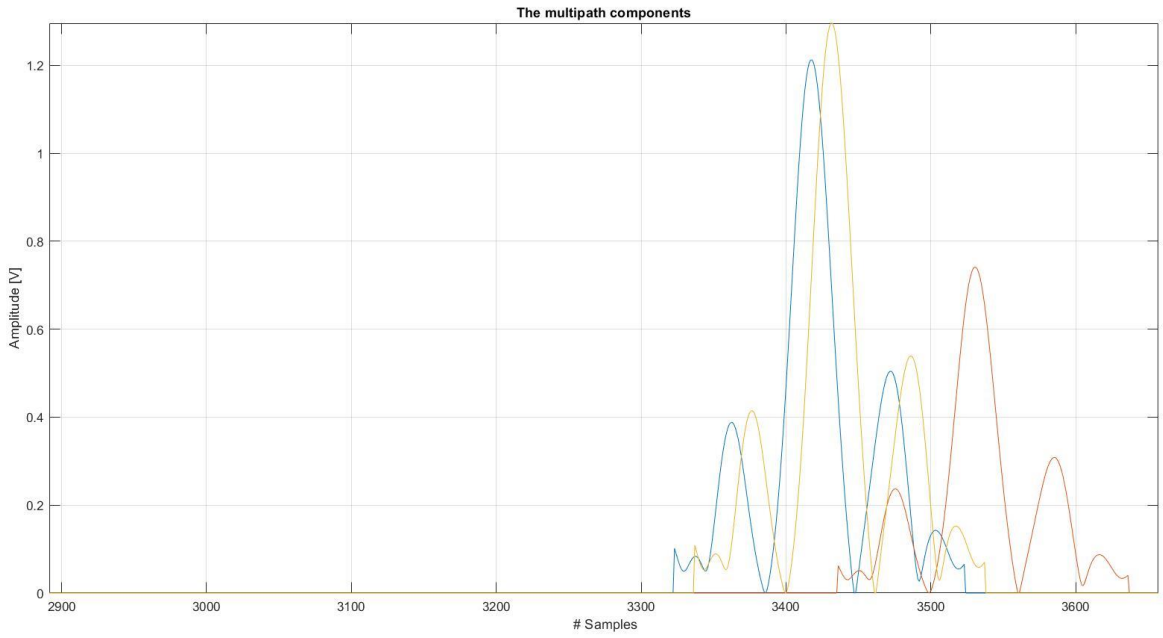

Figure 35 Wireless signal after SSR

Bibliography

[1] T. Kivinen, "datatracker.ietf.org," Internet Engineering Task Force (IETF), may 2017. [Online]. Available: https://datatracker.ietf.org/doc/html/rfc8137. [Accessed 15 06 2021].

[2] R. Yusnita, N. Razali, A. Tharek and H. P.S, "Ultra Wideband Technology and Its Applications," in *Wireless Communication Centre (WCC), Faculty of Electrical Engineering, Universiti Teknologi Malaysia 81310 Johor Bahru,Malaysia*, Department of Electronic, Electrical and Computer Engineering University of Birmingham Edgbaston Birmingham, B15 2TT United Kingdom.

[3] T. C. a. G. P. M. I. Marco Cavallaro, "Gaussian Pulse Generator for Millimeter-Wave," *IEEE TRANSACTIONS ON CIRCUITS AND SYSTEMS—I: REGULAR PAPERS, JUNE ,* Vols. NO. 6,VOL. 57, 2010.

[4] F. C. Commission, ""Revision of Part 15 of the Commission's Rules Regarding Ultra-Wideband Transmission Systems"," Fist Report and Order, ET Docket 98-153, FCC 02-48,April, 2002.

[5] I. Opperman, M. Hamalainen and J. Iinatti, UWB Theory and Applications, 2004.

[6] M. Andreas, "Ultra-Wide-Band Propagation Channels," in *Proceedings of IEEE*, 2009.

[7] A. Molisch, D. Cassioli, C.-C. Chong, S. Emami, A. Fort, B. Kannan, J. Karedak, J. Kunisch, H. Schantz, K. Siwiak and M. Win, "A Comprehensive Standardized Model for Ultrawideband Propagation Channels," *IEEE Transactions on Antennas and Propagation,* Vols. 54, no.11, 2006.

[8] V. C. Chen, F. Li, S.-S. Ho and H. Wechsler, "Micro-Doppler Effect in Radar: Phenomenon, Model and Simulation Study," *IEEE Transanctions on aerospace and electronic systems,* Vols. 42 , no. 1, 2006.

[9] J. Kwon, S. Lee and N. Kwak, "Human Detection by Deep Neural Networks Recognizing Micro-Doppler Signals of Radar," in *Proceedings of the 15th European Radar Conference* , 2018.

[10] V.-H. Nguyen and J.-Y. Pyun, "Location Detection and Tracking of Moving Targets by a 2D IR-UWB Radar System," *Sensors,* 2015.

[11] J.-H. Choi, J.-E. Kim and K.-T. Kim, "People Counting Using IR-UWB Radar Sensor in a Wide Area," *IEEE,* pp. 2327 - 4662, 2020.

[12] F. Diaconescu, "Impulse Radio UWB blind detectiong using Cross Recurrence Plot," in *2020 13th International Conference on Communications (COMM)*, Bucharest, Romania, 2020.

[13] S. Lim, J. Jung and S.-C. Kim, "Deep Neural Network-Based In-Vehicle People Localization Using Ultra-Wideband Radar," *IEEE ,* vol. 8, 2020.

[14] K. Youngwook and M. Taesup, "Human Detection and Activity Classification Based on Micro-Doppler Signatures Using Deep Convolutional Neural Networks," *IEEE GEOSCIENCE AND REMOTE SENSING LETTERS,* Vols. 13, NO. 1, January 2016.

[15] R. Qi, X. Li, Y. Zhang and Y. Li, "Multi-classification Algorithm for Human Motion Recognition Based on IR-UWB Radar," *IEEE Sensors Journal,* vol. 14, 2015.

[16] S. V. B. Joao, A. Zimmer and T. Brandmeier, "Pedestrian recognition using micro Doppler effects of radar signals based on machine learning and multi-objective optimization," *Expert Systems With Applications,* 2019.

[17] Y. Kim and H. Ling, "Human Activity Classification Based on Micro-Doppler Signatures Using a Support Vector Machine," *IEEE Transactions on Geoscience and Remote Sensing,* vol. 47, 2009.

[18] X. Yang, W. Yin, L. Li and L. Zhang, "Dense People Counting Using IR-UWB Radar with a Hybrid Feature Extraction Method," *IEEE Geoscience and Remote Sensing Letters,* vol. 16, no. 1, pp. 30-34, 2018.

[19] E. Candes , L. Demanet, D. Donoho and L. Ying, "Fast Discrete Curvelet Transforms," March 2006.

[20] M. Hozhabri, Human Detection and Tracking with UWB Radar, Stockholm: E-Print AB, 2019.

[21] C. SangHyun, M. Naoki and B. Joel, "An algorithm for UWB radar-based human detection," in *IEEE International Conference on Ultra-Wideband (ICUWB)*, Sydney, NSW, Australia doi:10.1109/ICUWB.2013.6663820, 2013.

[22] I. Oppermann, M. Hamalainen and J. Iinatti, UWB Theory and Applications, 2004.

[23] K. Yakup, W. Henk, M. Arjan, B. J. Mark and S. G. William, "An Experimental Study of UWB Device-Free Person Detection and Ranging," in *IEEE International Conference on Ultra-Wideband (ICUWB)*, Sydney, NSW, Australia doi:10.1109/ICUWB.2013.6663820, 2013.

[24] N. Van-Han and P. Jae-Young, "Location Detection and Tracking of Moving Targets by a 2D IR-UWB Radar System," *Sensors,* 2015.

[25] B. Schleicher and H. Schumacher, Impulse Generator Targeting the European UWB Mask, 2010.

[26] "A Summary of Worldwide Telecommunications Regulations governing the use of Ultra-Wideband radio," Decawave APPLICATION NOTE: APR001, 2015.

[27] I. Oppermann, M. Hamalainen and J. Iinatti, UWB Theory and Applications, 2004.

[28] L. Jing and Z. Zhaofa, "Through wall detection of human being's movement by UWB radar," in *The Society of Exploration Geophysicists to Chinese Geophysical Society*, Beijing, China, 2011.

[29] Q. Rui, L. Xiuping, Z. Yi and L. Yubing, "Multi-classification Algorithm for Human Recognition Based on IR-UWB Radar," *IEEE Sensors Journal,* Vols. 14, no. 8 , 2015.

[30] E. Anwar , S. Timothy, W. Safwan and X. Tian, "Machine Learning for Respiratory Detection Via UWB Radar Sensor".

[31] C. C. Victor , L. Fayin, H. Shen-Shyang and W. Harry, "Micro-Doppler Effect in Radar: Phenomenon, Model, and Simulation Study," *IEEE TRANSACTIONS ON AEROSPACE AND ELECTRONIC SYSTEMS,* Vols. 42,NO.1, 2006.

[32] A. Molisch, "Ultra-Wide-Band Propagation Channels," *Proceedings of the IEEE,* vol. 97, no. 2 DOI:10.1109/JPROC.2008.2008836, 2009.

[33] A. Molisch, "Ultra-Wide-Band Propagation Channels," in *Proceedings of the IEEE*, Vol.97 no. 2 2009.

[34] A. Molisch, D. Cassioli, C.-C. Chong, S. Emami, A. Fort, B. Kannan, J. Karedal, J. Kunisch, H. Schantz, K. Siwiak and M. Win, "A Comprehensive Standardized Model for Ultrawideband Propagation Channels," *IEEE Transactions on Antennas and Propagation,* vol. 54 no. 11, 2006.

[35] Z. Cui, Y. Gao, J. Hu, S. Tian and J. Cheng, "LOS/NLOS Identification for Indoor UWB Positioning Based on Morlet Wavelet Transform and Convolutional Neural Network," *IEEE Communications Letters,* 2020.

[36] F. Grejtak and A. Prokes, "UWB - ULTRA WIDEBAND CHARACTERISTICS AND THE SALEH-VALENZUELA," *Acta Electrotechnica et Informatica,* vol. 13 no. 2, p. 32–38, 2013.

[37] T. Ulrich, "Envelope Calculation from teh Hilbert Transform," March 2006.

[38] E.-T. Lee and H.-C. Eun, "Structural Damage Detection by Power Spectral Density Estimation Using Output-Only Measurement," *Hinwawi , Shock and Vibration,* 2016.

[39] J. C. Bancroft, "Introduction to matched filters," CREWES Research Rerport Volume 14, 2002.

[40] C. Falsi, D. Dardari, L. Mucchi and M. Win, "Time of Arrival Estimation for UWB Localizers in Realistic Environments," *EURASIP Journal on Applied Signal Processing,* vol. 2006, pp. 1-13.

[41] K. Jihoon, L. Seungeui and K. Nojun, "Human Detection by Deep Neural Networks Recognizing Micro-Doppler Signals of Radar," in *Proceedings of the 15th European Radar Conference*.

[42] D. Kocur, J. Gamec, M. Svecova, M. Gamcova and J. Rovnakova, "Imaginig Method: An efficient Algortihm for Moving Target Tracking by UWB Radar," *Acta Polytech.,* 2010.

[43] Z.-y. Zhang, X.-d. Zhang, H.-y. Yu and X.-h. Pan, "Noise suppression based on a fast discrete curvelet transform," *Journal of Geophysics and Engineering,* vol. 7, pp. 105-112, 2010.

[44] J. Fadili and J.-L. Starck, "Curvelets and Ridgelets," *R.A. Meyers, ed. Encyclopedia of Complexity and Systems Science ,* vol. 14, pp. 1718-1738, 2009.

[45] J. Ma and G. Plonka, "The Curvelet Transform," *IEEE Signal Processing Magazine,* 2010.

[46] Kassambara, "www.sthda.com," 23 09 2017. [Online]. Available: http://www.sthda.com/english/articles/31-principal-component-methods-in-r-practical-guide/112-pca-principal-component-analysis-essentials/. [Accessed 09 04 2021].

[47] Z. Jaadi, "https://builtin.com," 01 04 2021. [Online]. Available: https://builtin.com/data-science/step-step-explanation-principal-component-analysis. [Accessed 12 04 2021].

[48] "www.wikipedia.com," Wikipedia, 09 04 2021. [Online]. Available: https://en.wikipedia.org/wiki/Eigenvalues_and_eigenvectors. [Accessed 12 04 2021].

[49] S. Brunton and N. Kutz, Data-Driven Science and Engineering, Cambridge University Press,DOI: 10.1017/9781108380690, 2019.

[50] B. Schleicher and H. Schumacher , Impulse Generator Targeting the European UWB Mask, 2010.

[51] X. Guanlei, W. Xiaotong and X. Xiaogang, "Generalized Hilber transform and its properties in 2D LCT domain," *Signal Processing 89,* pp. 1395-1402, 2009.

[52] "www.wikipedia.com," 20 03 2021. [Online]. Available: https://en.wikipedia.org/wiki/Decision_tree. [Accessed 23 04 2021].

[53] B. Schleicher and H. Schumacher, Impulse Generator Targeting the European UWB Mask, 2010.

[54] F. Grejtak and A. Prokes, "UWB - ULTRA WIDEDBAND CHARACTERISTICS AND THE SALEH-VALENZUELA," *Acta Electrotehnica et Informatica,* vol. 13 . no. 2, pp. 32-38, 2013.